Computer Assisted Mechanics and Engineering Sciences, **13**: 523–536, 2006.

The influence of the microfibril angle on wood stiffness: a continuum micromechanics approach

Karin Hofstetter, Christian Hellmich, Josef Eberhardsteiner
Institute for Mechanics of Materials and Structures, Vienna University of Technology
Karlsplatz 13/202, 1040 Vienna, Austria

(Received in the final form October 6, 2006)

Wood exhibits an intrinsic structural hierarchy. It is composed of wood cells, which are hollow tubes oriented in the stem direction. The cell wall is built up by stiff cellulose fibrils which are embedded in a soft polymer matrix. This structural hierarchy is considered in a four-step homogenization scheme, predicting the macroscopic elastic behavior of different wood species from tissue-specific chemical composition and microporosity, based on the elastic properties of nanoscaled universal building blocks. Special attention is paid to the fact that the fibrils are helically wound in the cell wall, at an angle of 0°–30°, generally denoted as *microfibril angle*. Consideration of this microfibril angle in the continuum micromechanics model for wood is mandatory for appropriate prediction of macroscopic stiffness properties, in particular of the longitudinal elastic modulus and the longitudinal shear modulus. The presented developments can be readily extended to the prediction of poroelastic properties, such as Biot and Skempton coefficients.

Keywords: wood, continuum micromechanics, anisotropic elasticity, wood cell wall, experimental validation

1. Introduction

Macroscopic mechanical properties of wood are characterized by a wide variability and diversity [4, 32]. This variability results from differences observed at the macro-, micro-, and ultrastructural scale.

Wood is a cellular material with an intrinsic structural hierarchy [19, 32] as illustrated in Fig. 1. The wood cells are hollow tubes oriented in the stem direction (*longitudinal direction L*). In softwood, the cell diameter is typically around 20–40 μm, while in hardwood, there exist additional cells with up to 500 μm diameters, forming interconnected pipe-like structures called vessels. The cell wall is made up of cellulosic fibers with diameters of about 50–200 nm, embedded in a non-cellulosic matrix. The fibrils are helically wound around the lumens within the cell wall. The inclination angle of the fibers to the cell axis (*microfibril angle* $\bar{\theta}$, see Fig. 2) ranges between 0° and 30°. Only the inner core of a fibril is crystalline, while the surface region is more or less amorphous. The matrix deposited in the spaces between the cellulose is composed of non-cellulosic polysaccharides (commonly denoted as hemicelluloses), lignin, extractives, and inorganic compounds. In the wet state, water molecules interpenetrate the matrix. At higher water contents, water is also stored as free water in the cell lumens. The moisture content, at which the cell walls are saturated with bound water, but the cell lumens are still empty, is denoted as fiber saturation point. In the following, only wood tissues with water contents below this point are considered.

Predictions of the macroscopic mechanical behavior require consideration of the wood microstructure. The most common approach is that of cellular solids [21], which provides only very poor estimates of the elastic behavior with errors of more than 1000% between experimental values and theoretical estimates (see [21, p. 403, Fig. 10.12]. More detailed descriptions of the microstructure of wood, based on laminate theory for the representation of the internal structure of the cell wall [2, 44],

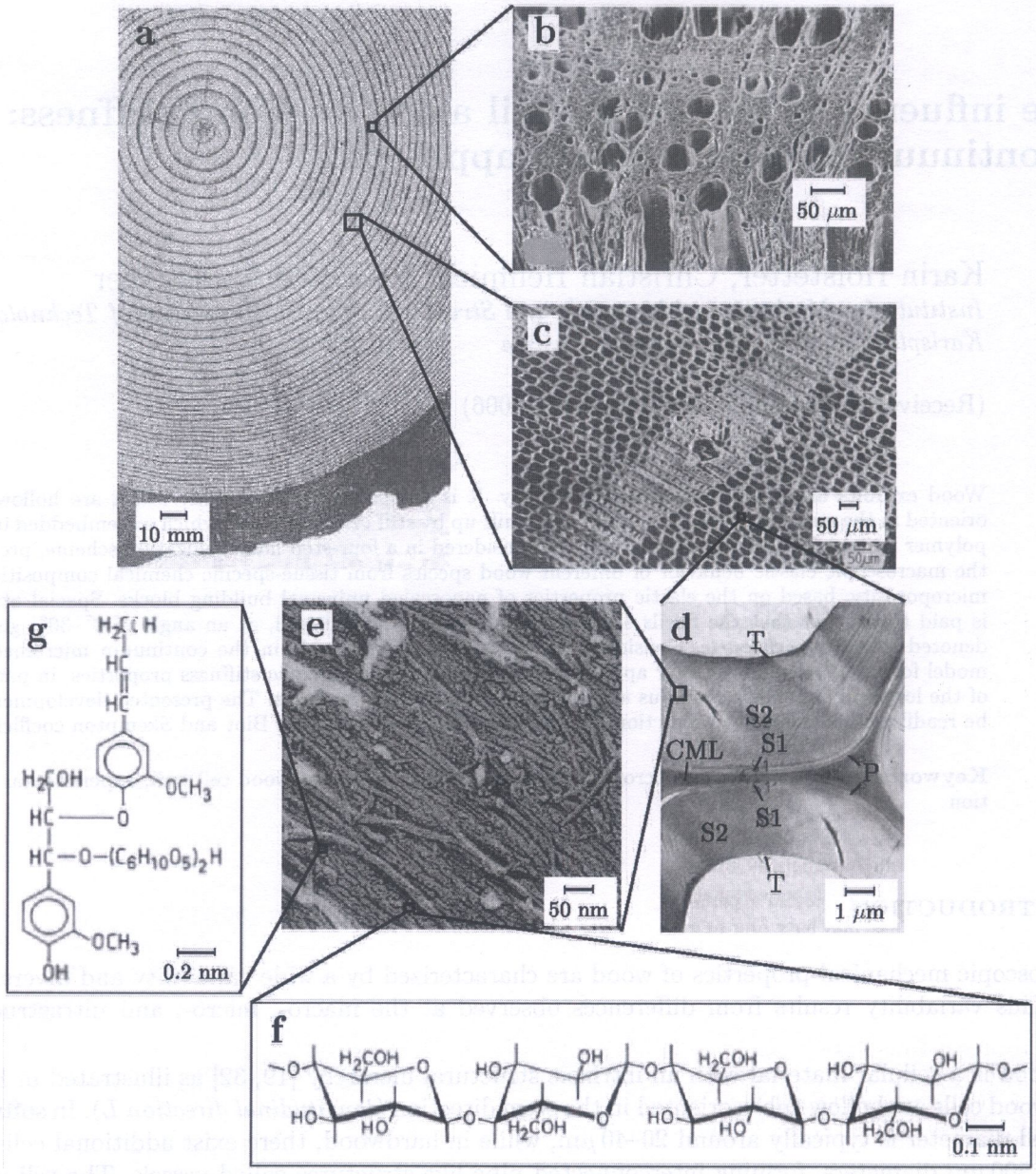

a Cross-section of a log (*Ponderosa pine*)[a]

b Transverse and longitudinal sections through a hardwood (*European beech*), Scanning electron micrograph (SEM)[b]

c Transverse section through a softwood (*Scots pine*), Scanning electron micrograph (SEM)[b]

d Section through the cell wall, showing the cell wall layers, Transmission electron micrograph (TEM)[b]

e Fibrillar structure of the S2 wall, Rapid freeze deep etching (RFDE) micrograph[c]

f Chemical structure of cellulose chain[b]

g Chemical structure of basic unit of a lignin-polysaccharide complex[b]

[a] From [43], permission for reproduction requested from Forest Product Society

[b] From [19], permission for reproduction requested from Kessel Verlag

[c] From [22], permission for reproduction requested from Oxford University Press

Fig. 1. Hierarchical organization of wood

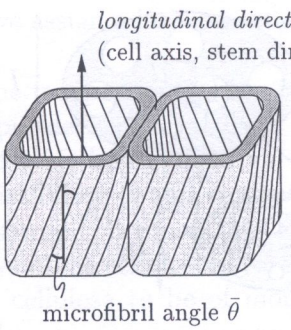

Fig. 2. Fibrillar (micro-)structure of wood cell wall

often require material parameters which lack a clear experimental basis. This limits the applicability of such models; in particular, it does not permit model predictions for non-tested conditions.

Thus, the authors invested in more reliable model predictions resting upon the method of continuum micromechanics [40, 46, 47]. In a first approach, the hierarchical structure of wood was represented by a four-step homogenization scheme [28], which is recalled in Section 2. A good agreement between model predictions and corresponding experimental results in terms of Young's moduli in the longitudinal and the transverse direction was obtained. This confirmed the suitability of the chosen approach as valuable tool for estimating the elastic properties of wood. Shear properties, however, were reproduced insufficiently by the micromechanical model, presumably due to the assumption of a zero microfibril angle. In detail, the axial straining of inclined fibers upon (macroscopic) shear loading of the composite material was disregarded. The crucial influence of the microfibril angle on the mechanical properties of wood has already been stressed by several authors, e.g. [8, 38].

Herein, we focus on consideration of the fiber inclination in the continuum micromechanics model.

2. Continuum micromechanics model

2.1. Fundamentals of continuum micromechanics

In continuum micromechanics [40, 47], a material is understood as a micro-heterogeneous body filling a representative volume element (RVE) with characteristic length l, $l \gg d$, d standing for the characteristic length of inhomogeneities within the RVE (see Fig. 3). The 'homogenized' mechanical behavior of the material, i.e. the relation between homogeneous deformations acting on the boundary of the RVE and resulting (average) stresses, can then be estimated from the mechanical behavior of different homogeneous phases (representing the inhomogeneities within the RVE), their dosages within the RVE, their characteristic shapes, and their interactions. Based on matrix-inclusion problems [17], an estimate for the 'homogenized' stiffness of a material reads as [47]

$$\mathbb{C}^{est} = \left\{ \sum_r f_r \, \mathbb{c}_r : \left[\mathbb{I} + \mathbb{P}_r^0 : (\mathbb{c}_r - \mathbb{C}^0) \right]^{-1} \right\} : \left\{ \sum_s f_s \left[\mathbb{I} + \mathbb{P}_s^0 : (\mathbb{c}_s - \mathbb{C}^0) \right]^{-1} \right\}^{-1}, \tag{1}$$

where $\mathbb{c}_r$ and f_r denote the elastic stiffness and the volume fraction of phase r, respectively, and $\mathbb{I}$, $I_{ijkl} = \frac{1}{2}(\delta_{il}\delta_{jk} + \delta_{ik}\delta_{jl})$, is the fourth-order unity tensor. The two sums are taken over all phases of the heterogeneous material in the RVE. The fourth-order tensor $\mathbb{P}_r^0$ accounts for the characteristic shape of phase r in a matrix with stiffness $\mathbb{C}^0$. Choice of this stiffness describes the interactions between the phases: For $\mathbb{C}^0$ coinciding with one of the phase stiffnesses (*Mori–Tanaka scheme*), a composite material is represented (contiguous matrix with inclusions); for $\mathbb{C}^0 = \mathbb{C}^{est}$ (*self-consistent scheme*), a dispersed arrangement of the phases is considered (typical for polycrystals). If a single phase exhibits a heterogeneous microstructure itself, its mechanical behavior can be

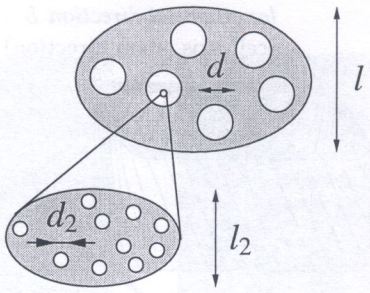

Fig. 3. Multistep homogenization

estimated by introduction of RVEs within this phase, with dimensions $l_2 \leq d$, comprising again smaller phases with characteristic length $d_2 \ll l_2$, and so on (see Fig. 3). This leads to a multistep homogenization scheme. Such a procedure should, in the end, provide access to 'universal' phase properties inherent to all wood tissues at a sufficiently low observation scale.

2.2. Candidates for (tissue-independent) micromechanical phases in wood

It follows from the aforementioned hierarchical organization that 'universal' properties inherent to all wood species may be identified only at an observation scale below the cell wall. Therefore, we lump its components (crystalline cellulose, amorphous cellulose, hemicellulose, lignin, extractives, inorganic compounds, and water) into as few phases as possible, characterized by remarkably differing elastic properties. The relevance of the subsequent candidates for universal phase properties (elementary components) inherent to all wood tissues will be checked in the validation section.

The first candidate for a tissue-independent ('universal') phase is amorphous cellulose. While we are not aware of elasticity measurements on amorphous cellulose, it is remarkable that glassy polymers with molecular structure similar to amorphous cellulose [13] exhibit Young's moduli of around 5 GPa [45]. Exploiting the similarity of the molecular structure of amorphous cellulose and hemicellulose, we assign a Poisson ratio of 0.35 to amorphous cellulose, which leads to the material properties given in Table 1. The amorphous nature of the material clearly suggests elastic isotropy.

Table 1. Experimental set I: 'Universal' (tissue-independent) phase stiffness values

Phase	Material behavior	Bulk modulus k [GPa]	Shear modulus μ [GPa]
Amorphous cellulose	isotropic	$k_{amocel} = 5.56$	$\mu_{amocel} = 1.85$
Hemicellulose	isotropic	$k_{hemcel} = 8.89$	$\mu_{hemcel} = 2.96$
Lignin	isotropic	$k_{lig} = 5.00$	$\mu_{lig} = 2.30$
Water+extract.	isotropic	$k_{H_2Oext} = 2.30$	$\mu_{H_2Oext} = 0$
		c_{ijkl} [GPa]	c_{ijkl} [GPa]
Crystalline cellulose	transversely isotropic	$c_{crycel,1111} = 34.86$ $c_{crycel,3333} = 167.79$	$c_{crycel,1122} = 0$ $c_{crycel,2233} = 0$ $c_{crycel,1313} = 5.81$

The second candidate for a tissue-independent phase is lignin. Periodate lignin[1] was shown to behave – in good approximation – isotropic in a uniaxial tension test [10], with Young's modulus of dry lignin amounting to slightly less than 6.7 GPa. This motivates a choice of 6 GPa for the elastic

[1]The term periodate lignin refers to the mode of extraction of the lignin from the cell wall [19]. Periodate lignin comes very close to in-situ lignin in terms of morphology and mechanical behavior.

modulus of lignin. Following [10], we assign a Poisson ratio of 0.3 to lignin, which leads to the phase properties given in Table 1.

The third candidate for a tissue-independent phase is hemicellulose. Cousins [11] tested rods made of (isotropic) hemicellulose powder extracted from Norway spruce by indentation with steel balls. Assuming a Poisson ratio of 0.35, he obtained an estimate of approximately 8 GPa for the elastic modulus of nearly dry hemicellulose (water content 1.51%) (see Table 1).

Since crystalline cellulose is anisotropic, it constitutes a fourth phase. Tashiro and Kobayashi [42] estimated the elastic stiffness of crystalline cellulose theoretically. They performed lattice-dynamical calculations, regarding crystalline cellulose to be of monoclinic crystal form. The corresponding stiffness tensor $\mathbb{C}^{mcl}_{crycel}$ reads as [42]

$$\mathbb{C}^{mcl}_{crycel} = \begin{bmatrix} \underset{(c_{1111})}{54.55} & \underset{(c_{1122})}{1.58} & \underset{(c_{1133})}{-2.52} & 0 & 0 & \underset{(c_{1112})}{-3.23} \\ & \underset{(c_{2222})}{15.16} & \underset{(c_{2233})}{1.26} & 0 & 0 & \underset{(c_{2212})}{4.31} \\ & & \underset{(c_{3333})}{167.79} & 0 & 0 & \underset{(c_{3312})}{0.51} \\ & & & \underset{(c_{2323})}{3.53} & \underset{(c_{2313})}{1.43} & 0 \\ & & & & \underset{(c_{1313})}{8.08} & 0 \\ & \text{symm.} & & & & \underset{(c_{1212})}{4.53} \end{bmatrix} \text{GPa}, \tag{2}$$

In Eq. (2), the third axis is aligned to the direction of the axes of the cellulose chains, whereas the first and second axes span the cross-sectional plane. The off-diagonal terms representing Poisson effects and coupling between shear and normal stress are remarkably smaller than the diagonal terms related to normal stress. Therefore, in a first approximation, Poisson effect and coupling between shear and normal stress can be neglected. The remaining components represent orthotropic elasticity. It stems from the sheet-like structures formed by cellulose chains connected by intermolecular hydrogen bonds. These sheets are, in turn, stacked together by van der Waals forces into a three-dimensional crystal, considerably softer in the direction of the van der Waals forces than in that of the hydrogen bonds within the sheets. The sheets are mainly aligned in the circumferential direction of the cell wall, so that, with regard to an entire cell, an even distribution of sheet orientations is encountered. This motivates the assumption of an isotropic material behavior in the cross-sectional plane of the cellulose chains, as also used by Bergander and Salmén [3]. The transverse isotropy may be considered by taking the average of the stiffness values in the principal cross-sectional directions of the monoclinic crystal,

$$c_{crycel,1111} = c_{crycel,2222} = \frac{1}{2}\left(c^{mcl}_{crycel,1111} + c^{mcl}_{crycel,2222}\right) = 34.86\,\text{GPa}, \tag{3}$$

$$c_{crycel,1313} = c_{crycel,2323} = \frac{1}{2}\left(c^{mcl}_{crycel,1313} + c^{mcl}_{crycel,2323}\right) = 5.81\,\text{GPa}\,. \tag{4}$$

The phase properties of crystalline cellulose are summarized in Table 1.

The term 'wood extractives' covers a large number of different compounds, which can be extracted from wood by means of water or organic solvents [19]. They are generally in the solute state, which motivates their common treatment with water in a fifth independent phase indicated by suffix 'H_2Oext'.

Inorganic compounds as, e.g., ash are only found in traces of typically 0.1–0.5 %. Given, in addition, their presumably insignificant stiffness, they hardly affect the mechanical properties of wood at a macroscopic scale. Hence, they are not regarded in the micromechanical model.

2.3. Continuum micromechanics model for wood

The interaction of the elementary components is considered in four homogenization steps (Fig. 4), which we describe in the following.

Polymer network

Within an RVE of polymer network with 8–20 nm characteristic length (see Fig. 4(a)), hemicellulose, lignin, and water are intimately mixed, occupying volume fractions $\tilde{f}_{hemcel}$, $\tilde{f}_{lig}$, and $\tilde{f}_{H_2Oext}$, $\tilde{f}_{hemcel} + \tilde{f}_{lig} + \tilde{f}_{H_2Oext} = 1$. The disorder of the chemical components in the network and the intimate mixing of the polymers and the water motivate the use of a self-consistent scheme with inclusions of spherical shape. Accordingly, in order to estimate the stiffness of the polymer network, $\mathbb{C}^{SCI}_{polynet}$, Eq. (1) is specified for three (spherical) inclusion phases, i.e. for $r \in [hemcel\,,\ lig\,,\ H_2Oext]$, for $\mathbb{C}_{hemcel}$, $\mathbb{C}_{lig}$, and $\mathbb{C}_{H_2Oext}$ according to Table 1, for $\mathbb{C}^0 = \mathbb{C}^{SCI}_{polynet}$, and for $\mathbb{P}^0_{hemcel} = \mathbb{P}^0_{lig} = \mathbb{P}^0_{H_2Oext} = \mathbb{P}^{polynet}_{sph}$, resulting in

$$\mathbb{C}^{SCI}_{polynet} = \left\{ \sum_r \tilde{f}_r \, \mathbb{C}_r : \left[\mathbb{I} + \mathbb{P}^{polynet}_{sph} : (\mathbb{C}_r - \mathbb{C}^{SCI}_{polynet}) \right]^{-1} \right\} : \\ : \left\{ \sum_s \tilde{f}_s \left[\mathbb{I} + \mathbb{P}^{polynet}_{sph} : (\mathbb{C}_s - \mathbb{C}^{SCI}_{polynet}) \right]^{-1} \right\}^{-1}, \\ r, s \in [hemcel\,,\ lig\,,\ H_2Oext]\,. \tag{5}$$

The elasticity tensors $\mathbb{C}_r$ of the isotropic phases are of the form

$$\mathbb{C}_r = 3\,k_r\,\mathbb{J} + 2\,\mu_r\,\mathbb{K}, \quad r \in [hemcel, lig, H_2Oext], \tag{6}$$

where k_r and μ_r are the bulk and shear moduli of the phases, $\mathbb{J}$, $J_{ijkl} = \frac{1}{3}\delta_{ij}\delta_{kl}$, is the volumetric part of the fourth-order unity tensor $\mathbb{I}$, and $\mathbb{K} = \mathbb{I} - \mathbb{J}$ is the deviatoric part. $\mathbb{P}^{polynet}_{sph}$ is of the form [24]

$$\mathbb{P}^{polynet}_{sph} = \mathbb{S}^{Esh,polynet} : \mathbb{C}^{SCI,-1}_{polynet}, \tag{7}$$

$$\mathbb{S}^{Esh,polynet} = \alpha^{SCI}_{polynet}\,\mathbb{J} + \beta^{SCI}_{polynet}\,\mathbb{K}, \tag{8}$$

with

$$\alpha^{SCI}_{polynet} = \frac{3\,k^{SCI}_{polynet}}{3\,k^{SCI}_{polynet} + 4\,\mu^{SCI}_{polynet}}, \qquad \beta^{SCI}_{polynet} = \frac{6\,(k^{SCI}_{polynet} + 2\,\mu^{SCI}_{polynet})}{5\,(3\,k^{SCI}_{polynet} + 4\,\mu^{SCI}_{polynet})}. \tag{9}$$

For implicit solution of Eq. (5), together with Eqs. (7)–(9), with respect to $\mathbb{C}^{SCI}_{polynet}$, we refer to Hellmich and coworkers [24, 25].

Cell wall material

Within an RVE of cell wall material with 0.5–1 μm characteristic length, cylindrical fiber-like aggregates of crystalline cellulose (with volume fraction f_{crycel}) and of amorphous cellulose (with volume fraction f_{amocel}), exhibiting typical diameters of 20–100 nm, are embedded in a contiguous polymer matrix (with volume fraction $f_{polynet} = 1 - f_{crycel} - f_{amocel}$). The behavior of such a composite material is suitably estimated by a Mori–Tanaka scheme. Accordingly, in order to estimate the stiffness of the cell wall material, $\mathbb{C}^{MTI}_{cwm}$, Eq. (1) is specified for two (cylindrical) inclusion phases (crystalline and amorphous cellulose) and one polymeric matrix phase, i.e. for $r \in [crycel\,,\ amocel\,,\ polynet]$,

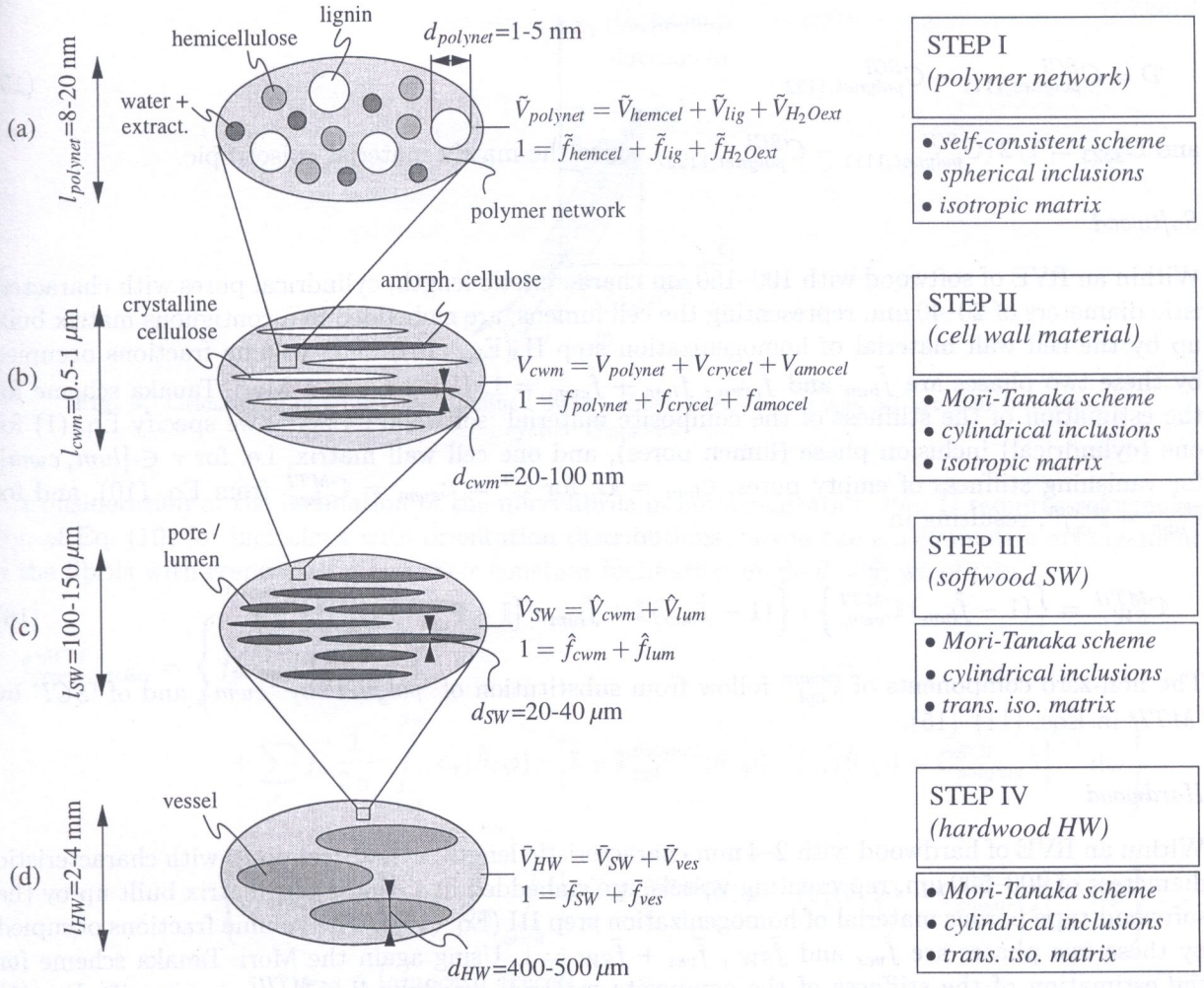

Fig. 4. Four-step homogenization procedure for wood

for $\mathbb{C}_{crycel}$ and $\mathbb{C}_{amocel}$ according to Table 1, for $\mathbb{C}^0 = \mathbb{C}_{polynet} = \mathbb{C}^{SCI}_{polynet}$ from Eq. (5), and for $\mathbb{P}^0_{crycel} = \mathbb{P}^0_{amocel} = \mathbb{P}^{polynet}_{cyl}$, resulting in

$$\mathbb{C}^{MTI}_{cwm} = \left\{ f_{polynet}\, \mathbb{C}^{SCI}_{polynet} + \sum_r f_r\, \mathbb{C}_r : \left[\mathbb{I} + \mathbb{P}^{polynet}_{cyl} : \left(\mathbb{C}_r - \mathbb{C}^{SCI}_{polynet} \right) \right]^{-1} \right\} : \left\{ f_{polynet}\, \mathbb{I} + \sum_s f_s : \left[\mathbb{I} + \mathbb{P}^{polynet}_{cyl} : \left(\mathbb{C}_s - \mathbb{C}^{SCI}_{polynet} \right) \right]^{-1} \right\}^{-1}, \quad (10)$$

$$r, s \in [crycel\,,\ amocel].$$

The non-zero components of the symmetric tensor $\mathbb{P}^{polynet}_{cyl}$ read as follows,

$$P^{polynet}_{cyl,1111} = P^{polynet}_{cyl,2222} = 1/8\,(5\,C^{SCI}_{polynet,1111} - 3\,C^{SCI}_{polynet,1122})/C^{SCI}_{polynet,1111}/\mathcal{D}, \quad (11)$$

$$P^{polynet}_{cyl,1122} = P^{polynet}_{cyl,2211} = -1/8\,(C^{SCI}_{polynet,1111} + C^{SCI}_{polynet,1122})/C^{SCI}_{polynet,1111}/\mathcal{D}, \quad (12)$$

$$P^{polynet}_{cyl,2323} = P^{polynet}_{cyl,1313} = 1/(8\,C^{SCI}_{polynet,2323}), \quad (13)$$

$$P^{polynet}_{cyl,1212} = 1/8\,(3\,C^{SCI}_{polynet,1111} - C^{SCI}_{polynet,1122})/C^{SCI}_{polynet,1111}/\mathcal{D}, \quad (14)$$

whereby

$$\mathcal{D} = C^{SCI}_{polynet,1111} - C^{SCI}_{polynet,1122} \tag{15}$$

and $C_{2323} = 1/2\,(C^{SCI}_{polynet,1111} - C^{SCI}_{polynet,1122})$, since the matrix material is isotropic.

Softwood

Within an RVE of softwood with 100–150 μm characteristic length, cylindrical pores with characteristic diameters of 20–40 μm, representing the cell lumens, are embedded in a contiguous matrix built up by the cell wall material of homogenization step II (Eq. (10)). The volume fractions occupied by these two phases are $\hat{f}_{lum}$ and $\hat{f}_{cwm}$, $\hat{f}_{lum} + \hat{f}_{cwm} = 1$. Using again a Mori–Tanaka scheme for the estimation of the stiffness of the composite material 'softwood', $\mathbb{C}^{MTII}_{SW}$, we specify Eq. (1) for one (cylindrical) inclusion phase (lumen pores), and one cell wall matrix, i.e. for $r \in [lum, cwm]$, for vanishing stiffness of empty pores, $\mathbb{c}_{lum} = \mathbb{O}$, for $\mathbb{C}^0 = \mathbb{c}_{cwm} = \mathbb{C}^{MTI}_{cwm}$ from Eq. (10), and for $\mathbb{P}^0_{lum} = \mathbb{P}^{cwm}_{cyl}$, resulting in

$$\mathbb{C}^{MTII}_{SW} = \left\{(1-\hat{f}_{lum})\,\mathbb{C}^{MTI}_{cwm}\right\} : \left\{(1-\hat{f}_{lum})\,\mathbb{I} + \hat{f}_{lum} : \left[\mathbb{I} - \mathbb{P}^{cwm}_{cyl} : \mathbb{C}^{MTI}_{cwm}\right]^{-1}\right\}^{-1}. \tag{16}$$

The non-zero components of $\mathbb{P}^{cwm}_{cyl}$ follow from substitution of '*polynet*' by '*cwm*', and of '*SCI*' by '*MTI*' in Eqs. (11)–(15).

Hardwood

Within an RVE of hardwood with 2–4 mm characteristic length, cylindrical pores with characteristic diameters of 400–500 μm, representing vessels, are embedded in a contiguous matrix built up by the softwood-type porous material of homogenization step III (Eq. (16)). The volume fractions occupied by these two phases are $\bar{f}_{ves}$ and $\bar{f}_{SW}$, $\bar{f}_{ves} + \bar{f}_{SW} = 1$. Using again the Mori–Tanaka scheme for the estimation of the stiffness of the composite material 'hardwood', $\mathbb{C}^{MTIII}_{HW}$, we specify Eq. (1) for one (cylindrical) inclusion phase (vessels), and one softwood-type matrix, i.e. for $r \in [ves, SW]$, for vanishing stiffness of empty vessels, $\mathbb{c}_{ves} = \mathbb{O}$, for $\mathbb{C}^0 = \mathbb{c}_{SW} = \mathbb{C}^{MTII}_{SW}$ from Eq. (16), and for $\mathbb{P}^0_{ves} = \mathbb{P}^{SW}_{cyl}$, resulting in

$$\mathbb{C}^{MTIII}_{HW} = \left\{(1-\bar{f}_{ves})\,\mathbb{C}^{MTII}_{SW}\right\} : \left\{(1-\bar{f}_{ves})\,\mathbb{I} + \bar{f}_{ves} : \left[\mathbb{I} - \mathbb{P}^{SW}_{cyl} : \mathbb{C}^{MTII}_{SW}\right]^{-1}\right\}^{-1}. \tag{17}$$

The non-zero components of $\mathbb{P}^{SW}_{cyl}$ follow from substitution of '*polynet*' by '*SW*', and of '*SCI*' by '*MTII*' in Eqs. (11)–(15).

3. Consideration of non-zero microfibril angles

3.1. Treatment of inclined inclusions in the framework of continuum micromechanics

The cellulose microfibrils are arranged in the wood cell wall in several concentric layers around the cell lumen [19]. The arrangement of the microfibrils is approximately axisymmetric at the observation scale of an entire cell [1]. The assumption of axisymmetry implies transverse isotropy of the material behavior of the cell wall, as in case of a zero microfibril angle.

The orientation of the microfibrils in a Cartesian coordinate system $Ox_1x_2x_3$ is defined by the Euler angles θ and φ (see Fig. 5). Provided that the x_3-axis is aligned with the axis of the wood cell, the angle θ corresponds to the microfibril angle.

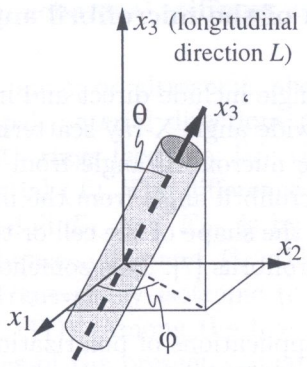

Fig. 5. Orientation of a microfibril defined by two Euler angles θ and φ in a Cartesian coordinate system $Ox_1x_2x_3$

Consideration of the inclination of the microfibrils in homogenization step II requires reformulation of Eq. (10) for inclusions with orientation distributions. Given the axisymmetric arrangement of the fibrils with respect to φ and their constant inclination angle $\theta = \bar{\theta}$, we obtain

$$\mathbb{C}^{MTI}_{cwm,inclin} = \left\{ f_{polynet}\, \mathbb{C}^{SCI}_{polynet} + \right.$$
$$\left. + \sum_r f_r \frac{1}{2\pi} \int_{\varphi=0}^{2\pi} \mathbb{C}_r(\bar{\theta},\varphi) : \left[\mathbb{I} + \mathbb{P}^{polynet}_{cyl}(\bar{\theta},\varphi) : \left(\mathbb{C}_r(\bar{\theta},\varphi) - \mathbb{C}^{SCI}_{polynet} \right) \right]^{-1} \mathrm{d}\varphi \right\} :$$
$$: \left\{ f_{polynet}\, \mathbb{I} + \sum_s f_s \frac{1}{2\pi} \int_{\varphi=0}^{2\pi} \left[\mathbb{I} + \mathbb{P}^{polynet}_{cyl}(\bar{\theta},\varphi) : \left(\mathbb{C}_s(\bar{\theta},\varphi) - \mathbb{C}^{SCI}_{polynet} \right) \right]^{-1} \mathrm{d}\varphi \right\}^{-1},$$
$$r, s \in [amocel\,,\ crycel]\,. \tag{18}$$

The fourth-order tensors $\mathbb{C}_r$ and $\mathbb{P}^{polynet}_{cyl}$ depend on the orientation of the inclusions. They are generally defined in a base frame $\mathbf{e}'_i$, $i = 1,2,3$, $\mathbf{e}'_i \cdot \mathbf{e}'_j = \delta_{ij}$, aligned with the axis of the (cylindrical) inclusion,

$$\mathbb{C}_r = (c_r)'_{ijkl}\, \mathbf{e}'_i \otimes \mathbf{e}'_j \otimes \mathbf{e}'_k \otimes \mathbf{e}'_l\,, \qquad \mathbb{P}^{polynet}_{cyl} = (P^{polynet}_{cyl})'_{ijkl}\, \mathbf{e}'_i \otimes \mathbf{e}'_j \otimes \mathbf{e}'_k \otimes \mathbf{e}'_l$$

(see [24] and [28] for mathematical details). The transformation of their components to the reference frame $\mathbf{e}_i$, $i = 1,2,3$, $\mathbf{e}_i \cdot \mathbf{e}_j = \delta_{ij}$,

$$\mathbb{C}_r = (c_r)_{ijkl}\, \mathbf{e}_i \otimes \mathbf{e}_j \otimes \mathbf{e}_k \otimes \mathbf{e}_l\,, \qquad \mathbb{P}^{polynet}_{cyl} = (P^{polynet}_{cyl})_{ijkl}\, \mathbf{e}_i \otimes \mathbf{e}_j \otimes \mathbf{e}_k \otimes \mathbf{e}_l\,,$$

requires standard rules of tensor calculus,

$$(c_r)_{ijkl} = n_{im}\, n_{jn}\, n_{kp}\, n_{lq}\, (c_r)'_{mnpq}\,, \qquad (P^{polynet}_{cyl})_{ijkl} = n_{im}\, n_{jn}\, n_{kp}\, n_{lq}\, (P^{polynet}_{cyl})'_{mnpq}\,, \tag{19}$$

where n_{im} denotes the cosine of the angle between the base vectors $\mathbf{e}_i$ and $\mathbf{e}'_m$. For bases $\mathbf{e}'_i$ and $\mathbf{e}_j$ rotated by Euler angles θ and φ, the tensor $\mathbf{n} = \{n_{ij}\}$ reads in matrix notation as

$$\mathbf{n} = \begin{bmatrix} \cos(\varphi) & -\sin\varphi & 0 \\ \cos(\theta)\,\sin(\varphi) & \cos(\theta)\,\cos(\varphi) & -\sin(\theta) \\ \sin(\theta)\,\sin(\varphi) & \sin(\theta)\,\cos(\varphi) & \cos(\theta) \end{bmatrix}. \tag{20}$$

The integrals in Eq. (18) are evaluated numerically, the integral being replaced by a sum.

3.2. Experimental determination of the microfibril angle

Methods to measure the microfibril angle include direct and indirect techniques. The most popular indirect method is X-ray scattering (wide angle X-ray scattering [6, 18] and small angle X-ray scattering [30, 33, 37]), which derives the microfibril angle from diffraction patterns of irradiated cell wall sections. Computation of the microfibril angle from the measured radiation intensities requires several assumptions, concerning, e.g., the shape of the cell or the orientation of the cellulose crystallites with respect to the cellulose microfibrils [7]. This somehow limits the quantitative significance of such test results.

Direct methods include different applications of polarization microscopy (PM) [12, 14], staining methods (SM) [15, 27], or examination of the direction of iodine crystals (IC) [39] or of soft rot cavities [31]. Providing direct access to the microfibril angle, these methods provide data free of any manipulation during evaluation. Results of microfibril angle measurements by means of direct methods indicate a mean angle of 20° for the wood cell wall of different species (cf. Table 2).

Table 2. Microfibril angle (MFA) measurements for different wood species by means of direct methods

Species	Meth.	MFA [°]	Reference
Spruce	PM	18.1–20.4	[35]
	PM	25.5	[36]
	SM	13–17	[15]
Pine	SM	4–40	[27]
	PM	20	[34]
	PM	17–24	[41]
	PM	12–27	[5]
	PM	20	[23]
Douglas fir	SM	13–28	[15]
	PM	7–30	[16]
	IC	10–30	[20]
Hemlock	SM	17–22	[15]

4. Validation

The validation of the micromechanical model is based on two independent sets of experimental data (see e.g. [24] and [28]): Micromechanical stiffness estimates based on tissue-independent phase stiffness properties of hemicellulose, $\mathbb{C}_{hemcel}$, of lignin, $\mathbb{C}_{lig}$, of water lumped together with extractives, $\mathbb{C}_{H_2Oext}$, of amorphous cellulose, $\mathbb{C}_{amocel}$, and of crystalline cellulose, $\mathbb{C}_{crycel}$, [experimental set I, Subsection 2.2 and Table 1] as well as on tissue and sample-dependent composition data in terms of volume fractions f_{hemcel}, f_{lig}, f_{H_2O}, f_{ext}, f_{amocel}, f_{crycel}, f_{lum}, and f_{ves}, [experimental set IIa] are compared to corresponding experimentally determined stiffness values [experimental set IIb]. The volume fractions are derived from chemical analysis, microscopic methods, and X-ray diffraction as described in [28], with a degree of crystallinity of cellulose of 0.66, in agreement with many textbooks on wood (e.g. [19, 32]).

The stiffness values are derived either from quasi-static (tension or compression) tests, or from dynamic tests, in which the free bending vibration of wood specimens is examined, or from ultrasonic tests, in which propagation velocities of ultrasonic waves are measured, allowing for computation of the components of the elastic stiffness tensor. A large number of wood tissues, from a variety of softwood and hardwood species, are considered, see [28] for details.

4.1. Comparison between micromechanical stiffness estimates and experimental values

Mechanical tests, be they static, dynamic, or ultrasonic, show the orthotropy of the elasticity of hardwood and softwood. The principal material directions coincide with the stem axis and with the normal and tangent of the growth rings (see Fig. 1a); they are standardly referred to as longitudinal (L), radial (R), and tangential (T). The difference between the axial and the transverse properties, e.g. between Young's moduli E_L and E_R, is by far larger than that between the radial and tangential properties, e.g. between E_R and E_T. Therefore, it seems sensible to consider wood, in a first approximation, as transversely isotropic (cf. the transversely isotropic estimates $\mathbb{C}_{SW}^{MTII}$ and $\mathbb{C}_{HW}^{MTIII}$ in Eqs. (16) and (17)). Among the five independent elastic constants derived from the experimental data, the focus of the present validation is on Young's moduli in the axial (longitudinal) and in the transverse direction, E_L and $E_{trans} = 1/2\,(E_R + E_T)$, and on the longitudinal shear modulus, $G_L = 1/2\,(G_{LR} + G_{LT})$. Micromechanical stiffness predictions for the elastic moduli E_L^{pred} and E_{trans}^{pred}, $E_L^{pred} = 1/[\mathbb{C}_{HW}^{MTIII,-1}]_{3333}$, $E_{trans}^{pred} = 1/[\mathbb{C}_{HW}^{MTIII,-1}]_{1111}$ for hardwood and $E_L^{pred} = 1/[\mathbb{C}_{SW}^{MTII,-1}]_{3333}$, $E_{trans}^{pred} = 1/[\mathbb{C}_{SW}^{MTII,-1}]_{1111}$ for softwood, and for the shear modulus G_L^{pred}, $G_L^{pred} = C_{HW,1313}^{MTIII}$ for hardwood and $G_L^{pred} = C_{SW,1313}^{MTII}$ for softwood, based on non-deviating and deviating microfibrils ($\bar{\theta} = 0°, 20°$), are compared to corresponding experimental measurements (see Fig. 6). Each pair of stiffness measurement and corresponding micromechanical prediction is indicated by a wood species-specific marker. The solid lines indicate perfect agreement between predicted and experimental stiffness values.

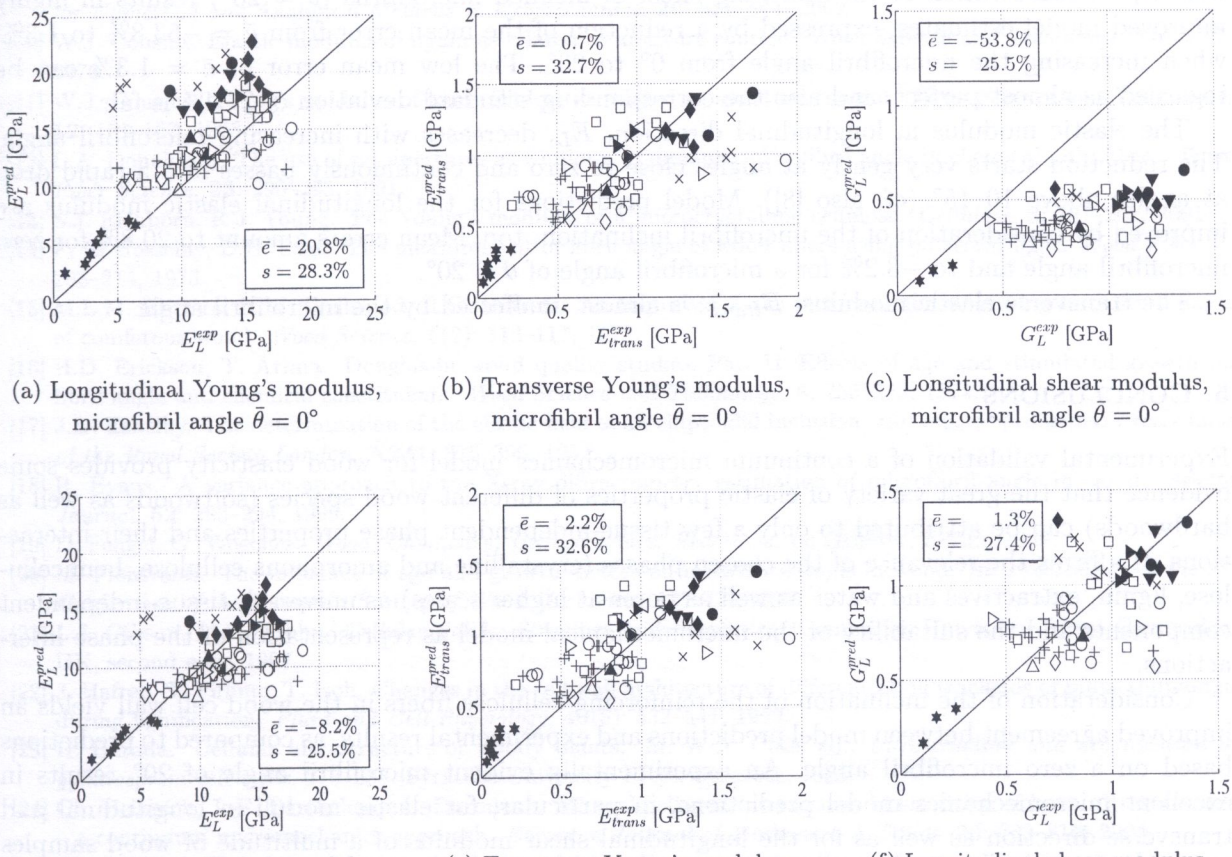

(a) Longitudinal Young's modulus, microfibril angle $\bar{\theta} = 0°$

(b) Transverse Young's modulus, microfibril angle $\bar{\theta} = 0°$

(c) Longitudinal shear modulus, microfibril angle $\bar{\theta} = 0°$

(d) Longitudinal Young's modulus, microfibril angle $\bar{\theta} = 20°$

(e) Transverse Young's modulus, microfibril angle $\bar{\theta} = 20°$

(f) Longitudinal shear modulus, microfibril angle $\bar{\theta} = 20°$

Fig. 6. Comparison of predicted and measured elastic constants for non-deviating and deviating microfibrils; ◇ Cedar, ○ Douglas Fir, △ Fir, ▷ Hemlock, ◁ Larch, □ Pine, + Spruce, ♦ Ash, ∗ Balsa, • Beech, ▶ Birch, ▼ Maple, × Oak, ▲ Poplar

To quantify the predictive capabilities of the micromechanical model, differences between predicted micromechanical stiffness estimates and experimental measurements are determined in terms of mean values and standard deviations of absolute errors $\bar{E}$ and S, reading for n pairs (X_i^{pred}, X_i^{exp}) of model predictions and experimental results as

$$\bar{E} = \frac{1}{n}\sum_{i=1}^{n}\left(X_i^{pred} - X_i^{exp}\right) = \frac{1}{n}\sum_{i=1}^{n} E_i\,, \qquad S = \left[\frac{1}{n-1}\sum_{i=1}^{n}(E_i - \bar{E})^2\right]^{1/2}. \tag{21}$$

These error measurements are normalized with respect to the mean value of all experimental results

$$\bar{X}^{exp} = \frac{1}{n}\sum_{i=1}^{n} X_i^{exp}\,, \tag{22}$$

yielding the error measures $\bar{e}$ and s in the form

$$\bar{e} = \frac{\bar{E}}{\bar{X}^{exp}}\,, \qquad s = \frac{S}{\bar{X}^{exp}}\,. \tag{23}$$

Error measures for the pairs of model predictions and experimental results considered in the model validation, obtained with either zero or non-zero microfibril angle, are included in Fig. 6. They are based on 118 samples of 16 different species for E_L, on 84 samples of 14 different species for E_{trans}, and on 73 samples of 14 different wood species for G_L.

The influence of the microfibril angle is specially pronounced for the longitudinal shear modulus G_L. Consideration of the stiffening effect of inclined microfibrils ($\bar{\theta} = 20°$) results in highly improved model estimates, expressed by a reduction of the mean error from $\bar{e} = -53.8\%$ to 1.3%, when increasing the microfibril angle from 0° to 20°. The low mean error of $\bar{e} = 1.3\%$ can be regarded as almost perfect, and also the corresponding standard deviation of 27.4% is fair.

The elastic modulus in longitudinal direction, E_L, decreases with increasing microfibril angle. The reduction starts very gently at angles close to zero and continuously passes into a rapid drop at angles above 10–15° (cf. also [8]). Model predictions for the longitudinal elastic modulus are improved by consideration of the microfibril inclination, too. Mean errors amount to 20.8% for zero microfibril angle and to −8.2% for a microfibril angle of $\theta = 20°$.

The transverse elastic modulus, E_{trans}, is almost unaffected by the microfibril angle.

5. Conclusions

Experimental validation of a continuum micromechanics model for wood elasticity provides some evidence that the great variety of elastic properties of different wood species (softwoods as well as hardwoods) can be attributed to only a few tissue-independent phase properties and their interactions. It affirms the relevance of the chosen phases (crystalline and amorphous cellulose, hemicellulose, lignin, extractives and water as well as pores at higher scales) as universal, tissue-independent components and the suitability of the micromechanical model as representation of the phase interactions.

Consideration of the inclination of the reinforcing cellulose fibers in the wood cell wall yields an improved agreement between model predictions and experimental results, as compared to predictions based on a zero microfibril angle. An experimentally evident microfibril angle of 20° results in excellent micromechanics model predictions, in particular, for elastic moduli in longitudinal and transverse direction as well as for the longitudinal shear modulus of a multitude of wood samples of different softwood and hardwood species. The small mean values of the corresponding relative errors between model predictions and experimental results, together with a fair standard deviation of these errors, indicate that the microstructure of wood cells can be suitably characterized by a single microfibril angle valid for different wood species, at least with respect to prediction of macroscopic elastic properties. The influence of the microfibril angle is especially striking for the longitudinal

shear modulus. In particular, model validation elucidates that longitudinal shear stiffness of wood is largely due to axial straining of the cellulose fibers inclined towards the longitudinal stem axis.

The elasticity model constitutes a basis for prediction of the elastic limit of wood [29] and, in future research, of poroelastic properties [9, 26]. This will open the door to applications of the model in wood drying technology and in timber construction design.

REFERENCES

[1] A. Bergander. *Local variability in chemical and physical properties of spruce wood fibers.* Doctoral Thesis, KTH Stockholm, 2001.

[2] A. Bergander, L. Salmén. Variations in transverse fibre wall properties: Relations between elastic properties and structure. *Holzforschung*, **54**: 654–660, 2000.

[3] A. Bergander, L. Salmén. Cell wall properties and their effect on the mechanical properties of fibers. *Journal of Material Science*, **37**: 151–156, 2002.

[4] J. Bodig, B.A. Jayne. *Mechanics of Wood and Wood Composites.* Van Nostrand Reinhold, New York, USA, 1982.

[5] J.D. Boyd, R.C. Foster. Microfibrils in primary and secondary wall growth develop trellis configurations. *Canadian Journal of Botany*, **53**(23): 2687–2701, 1975.

[6] I.D. Cave. Theory of X-ray measurement of microfibril angle in wood. *Forest Products Journal*, **16**: 37–42, 1966.

[7] I.D. Cave. Theory of X-ray measurement of microfibril angle in wood. Part I. The diffraction diagramm X-ray diffraction by materials with fibre type symmetry. *Wood Science and Technology*, **37**: 225–234, 1997.

[8] I.D. Cave, J.C.F. Walker. Stiffness of wood in fast-grown plantation softwoods: the influence of microfibril angle. *Forest Products Journal*, **44**(5): 43–48, 1994.

[9] X. Chateau, L. Dormieux. Micromechanics of saturated and unsaturated porous media. *International Journal for Numerical and Analytical Methods in Geomechanics*, **26**: 831–844, 2002.

[10] W.J. Cousins. Elastic modulus of lignin as related to moisture content. *Wood Science and Technology*, **10**: 9–17, 1976.

[11] W.J. Cousins. Young's modulus of hemicellulose as related to moisture content. *Wood Science and Technology*, **12**: 161–167, 1978.

[12] L.A. Donaldson. The use of pit apertures as windows to measure microfibril angle in chemical pulp fibres. *Wood Fiber Science*, **23**: 290–295, 1991.

[13] S.J. Eichhorn, R.J. Young. The Young's modulus of a microcrystalline cellulose. *Cellulose*, **8**: 197–207, 2001.

[14] F. El-Hosseiny, D.H. Page. The measurement of fibril angle of wood fibers using polarized light. *Wood Fiber*, **5**: 208–214, 1973.

[15] M.L.M. El-Osta, R.W. Wellwood, R.G. Butters. An improved X-ray technique for measuring microfibril angle of coniferous wood. *Wood Science*, **5**(2): 113–117, 1972.

[16] H.D. Erickson, T. Arima. Douglas-fir wood quality studies. Part II: Effects of age and stimulated growth on fibril angle and chemical constituents. *Wood Science and Technology*, **8**: 255–265, 1974.

[17] J.D. Eshelby. The determination of the elastic field of an ellipsoidal inclusion, and related problems. *Proceedings of the Royal Society London*, **A241**: 376–396, 1957.

[18] R. Evans. A variance approach to the X-ray diffractometry estimation of microfibril angle in wood. *Appita Journal*, **52**: 283–294, 1999.

[19] D. Fengel, G. Wegener. *Wood. Chemistry, Ultrastructure, Reactions.* de Gruyter, Berlin, 1989.

[20] M. Fioravanti. The influence of age and growth factors on microfibril angle in wood. In: *Proceedings of the* 1^{st} *Conference of the European Society of Wood Mechanics*, 127–134, 2001.

[21] L.J. Gibson, M.F. Ashby. *Cellular Solids. Structure and Properties.* Cambridge University Press, Cambridge, UK, second edn., 1997.

[22] J. Hafren, T. Fujimo, T. Itoh. Changes in the cell wall architecture of differentiating tracheids of pinus thunbergii during lignification. *Plant and Cell Physiology*, **40**(5): 532–541, 1999.

[23] H. Harada. Cellular ultrastructure of woody plants. In: W.A. Côté, ed., *Ultrastructure and organization of gymnosprem cell walls*, 215–233. Syracuse University Press, Syracuse, 1965.

[24] Ch. Hellmich, J.-F. Barthélémy, L. Dormieux. Mineral-collagen interactions in elasticity of bone ultrastructure – a continuum micromechanics approach. *European Journal of Mechanics A/Solids*, **23**: 783–810, 2004.

[25] Ch. Hellmich, F.-J. Ulm. Micromechanical model for ultrastructural stiffness of mineralized tissues. *Journal of Engineering Mechanics (ASCE)*, **128**(8): 898–908, 2002.

[26] Ch. Hellmich, F.-J. Ulm. Drained and undrained poroelastic properties of healthy and pathological bone: A poro-micromechanical investigation. *Transport in Porous Media*, **58**(3): 243–268, 2005.

[27] C.H. Hiller. Correlation of fibril angle with wall thickness of tracheids in summerwood of slash and loblolly pine. *Tappi*, **47**(2): 125–128, 1964.

[28] K. Hofstetter, Ch. Hellmich, J. Eberhardsteiner. Develpoment and experimental validation of a continuum micromechanics model for the elasticity of wood. *European Journal of Mechanics A/Solids*, **24**: 1030–1053, 2005.

[29] K. Hofstetter, Ch. Hellmich, J. Eberhardsteiner. Wood strength properties predicted from microstructure and composition: a continuum micromechanics approach. *European Journal of Mechanics A/Solids*, 2006. Submitted for publication.

[30] H.F. Jakob, P. Fratzl, S.E. Tschegg. Size and arrangement of elementary cellulose fibrils in wood cells: A Small-Angle X-Ray Scattering study of Picea Abies. *Journal of Structural Biology*, **113**: 13–22, 1994.

[31] S. Khalili, T. Nilsson, G. Daniel. The use of soft rot fungi for determining the microfibrillar orientation in the s2 layer of pine tracheids. *Holz als Roh- und Werkstoff*, **58**: 439–447, 2001.

[32] F. Kollmann, W. Côté. *Principles of Wood Science and Technology*, Vol. 1. Springer Verlag, Berlin, Heidelberg, New York, 1968.

[33] H. Lichtenegger, A. Reiterer, S.E. Stanzl-Tschegg, P. Fratzl. Variation of cellulose microfibril angles in softwoods and hardwoods – a possible strategy of mechanical optimization. *Journal of Structural Biology*, **128**: 257–269, 1999.

[34] R.E. Mark. *Cell wall mechanics of tracheids*. Yale University Press, New Haven, USA, 2 edn., 1967.

[35] R. Marton, S.D. McGovern. Relation of the crystallite dimensions of fibrillar orientation to fiber properties. In: *The physics and chemistry of wood pulp fibers*, 153–158. Tappi stap No. 8, 1970.

[36] P.J. Ollinmaa. Reaktiopuututkimuksai. *Acta Forestalia Fennica*, **72**, 1961.

[37] A. Reiterer, H.F. Jakob, S.E. Tschegg, P. Fratzl. Spiral angle of elementary cellulose fibrils in cell walls of picea abies determined by small-angle X-ray scattering. *Wood Science and Technology*, **43**(5): 335–345, 1998.

[38] A. Reiterer, H. Lichtenegger, S. Tschegg, P. Fratzl. Experimental evidence for a mechanical function of the cellulose microfibril angle in wood cell walls. *Philosophical Magazine A*, **79**(9): 2173–2184, 1999.

[39] J.F. Senft, B.A. Bendtsen. Measuring microfibrillar angles using light microscopy. *Wood Fiber Science*, **17**: 564–567, 1985.

[40] P. Suquet, ed. *Continuum Mircomechanics*. Springer Verlag, Wien, New York, 1997.

[41] R.C. Tang. The microfibrillar orientation in cell-wall layers of virginia pine tracheids. *Wood Science and Technology*, **5**: 181–186, 1973.

[42] K. Tashiro, M. Kobayashi. Theoretical evaluation of three-dimensional elastic constants of native and regenerated celluloses: role of hydrogen bonds. *Polymer*, **32**(8): 1516–1526, 1991.

[43] WHB. *Wood Handbook*. Forest Products Society, USA, 1999.

[44] H. Yamamoto, Y. Kojima, T. Okuyama, W.P. Abasolo, J. Gril. Origin of the biomechanical properties of the fine structure of the multi-layered cell wall. *Journal of Biomechanical Engineering (ASME)*, **124**: 432–440, 2002.

[45] R.J. Young, P.A. Lovell. *Introduction to Polymers*. Chapman & Hall, London, 2 edn., 1991.

[46] A. Zaoui. Structural morphology and constitutive behavior of microheterogeneous materials. In: P. Suquet, ed., *Continuum Micromechanics*, 291–347. Springer Verlag, Wien, New York, 1997.

[47] A. Zaoui. Continuum micromechanics: Survey. *Journal of Engineering Mechanics (ASCE)*, **128**(8): 808–816, 2002.